High-Pressure Synthesis, Crystal Structure, and Properties of the New Orthorhombic Rare-Earth *meta*-Oxoborates $RE(BO_2)_3$ (RE = Dy – Lu)

Holger Emme[a], Tanja Nikelski[b], Thomas Schleid[b], Rainer Pöttgen[c], Manfred Heinrich Möller[c], and Hubert Huppertz[a]

[a] Department Chemie, Ludwig–Maximilians–Universität München, Butenandtstraße 5–13 (Haus D), D-81377 München, Germany
[b] Institut für Anorganische Chemie der Universität Stuttgart, Pfaffenwaldring 55, D-70550 Stuttgart, Germany
[c] Institut für Anorganische und Analytische Chemie, Universität Münster, Wilhelm-Klemm-Straße 8, D-48149 Münster, Germany

Reprint requests to Dr. H. Huppertz. E-mail: huh@cup.uni-muenchen.de

Z. Naturforsch. **59b,** 202 – 215 (2004); received December 22, 2003

Dedicated to Professor Ingo-Peter Lorenz on the occasion of his 60th birthday

The new orthorhombic *meta*–oxoborates $RE(BO_2)_3$ ($\equiv REB_3O_6$) (RE = Dy–Lu) have been synthesized under high-pressure and high-temperature conditions in a Walker-type multianvil apparatus at 7.5 GPa and 1100 °C. They are isotypic to the known ambient pressure phase $Tb(BO_2)_3$, space group *Pnma*. In contrast to $Dy(BO_2)_3$, which was also obtained in small amounts under high-temperature conditions, the preparation of the higher orthorhombic homologues $RE(BO_2)_3$ (RE = Ho–Lu) was only possible using high-pressure. The *meta*-oxoborates $RE(BO_2)_3$ (RE = Dy–Er) were synthesized as pure products, whereas the orthorhombic phases with RE = Tm–Lu were only obtained as byproducts. With the exception of $Yb(BO_2)_3$ it was possible to establish single crystal data for all compounds. The results of temperature-resolved *in-situ* powder-diffraction measurements, DTA, IR-spectroscopic investigations, and magnetic properties are also presented.

Key words: High-Pressure, Oxoborates, Crystal Structure

Introduction

The class of oxoborates has been investigated extensively in the past decades, owing to their structural aspects and interesting physical properties, *e. g.* NLO (non-linear optics) and fluorescence [1 – 4]. In the system RE_2O_3–B_2O_3 the fundamental series of compounds with the molar ratios 1:1 [5 –23], 1:3 [24 – 33], and 3:1 [16] were recently extended by compositions 2:7 [34], 1:5 [35], $\sim$ 8.7:4 [36, 37], and 13:4 [38]. Using high-pressure as an additional parameter, it was possible to enlarge the range of attainable compositions by the ratios 2:3 [39, 40] and 1:2 [41 – 43] with the formulas $RE_4B_6O_{15}$ (RE = Dy, Ho), α-$RE_2B_4O_9$ (RE = Eu, Gd, Tb, Dy), and β-$RE_2B_4O_9$ (RE = Dy). In the last months, the *meta*-oxoborates (1:3) especially, were examined again by Held *et al.* [32] and Schleid *et al.* [31 – 33]. In these investigations, the monoclinic phase $Gd(BO_2)_3$ ($\equiv GdB_3O_6$; $a = 973.4(8)$, $b = 802.7(5)$, $c = 629.6(5)$ pm, $\beta = 126.84(1)°$) [29, 44] marked the end of a series of well characterized monoclinic *meta*-oxoborates $RE(BO_2)_3$ (RE = La, Nd, Sm, Gd). Recently, Schleid *et al.* synthesized the *meta*-oxoborate $Tb(BO_2)_3$ and solved its orthorhombic crystal structure (*Pnma*, $a = 1598.97(9)$, $b = 741.39(4)$, $c = 1229.58(7)$ pm) [31]. $Tb(BO_2)_3$ was obtained by the reaction of metallic terbium, Tb_4O_7, and $TbCl_3$ with an excess of B_2O_3 in gastight sealed platinum ampoules at 950 °C after three weeks. Interestingly, Held *et al.* were able to synthesize the monoclinic polymorph of $Tb(BO_2)_3$ using a homogenized powder mixture of Tb_4O_7, H_3BO_3, and PbO in a molar ratio of 1.1 : 87.9 : 11.0 at 940 °C in a covered platinum crucible with the *in-situ* generated lead borate acting as a flux [32]. Additional experiments by Schleid *et al.* showed that of the higher rare earth homologues (Dy–Lu) only the dysprosium compound can be synthesized under the mentioned conditions. Less is known about the higher homologues of the metaborates REB_3O_6 (RE = Ho–Lu). In 1975, Tananaev *et al.* synthesized these compounds starting from RE_2O_3, B_2O_3, and Na_2O as a flux-material [28]. On the basis

0932–0776 / 04 / 0200–0202 $ 06.00 © 2004 Verlag der Zeitschrift für Naturforschung, Tübingen · http://znaturforsch.com

Table 1. Crystal data and structure refinement for $RE(BO_2)_3$ (RE = Dy, Ho, Er).

Empirical formula	DyB_3O_6	HoB_3O_6	ErB_3O_6
Molar mass [g·mol^{-1}]	290.93	293.36	295.69
Crystal system		orthorhombic	
Space group		*Pnma* (Nr. 62)	
Powder diffractometer		Stoe Stadi P	
Radiation		Cu-K$_{\alpha 1}$ ($\lambda = 154.06$ pm)	
Powder diffraction data			
a [pm]	1592.4(1)	1590.0(4)	1589.1(2)
b [pm]	739.7(1)	739.3(2)	737.6(1)
c [pm]	1225.0(1)	1223.1(4)	1219.1(1)
Volume [nm^3]	1.443(1)	1.437(1)	1.429(1)
Single crystal diffractometer		Enraf-Nonius Kappa CCD	
Radiation		Mo-K$_\alpha$ ($\lambda = 71.073$ pm)	
Single crystal data			
a [pm]	1593.0(2)	1591.9(2)	1587.6(2)
b [pm]	740.2(2)	739.5(2)	738.0(2)
c [pm]	1226.4(2)	1223.3(2)	1218.9(2)
Volume [nm^3]	1.446(1)	1.440(1)	1.428(1)
Formula units per cell		$Z = 16$	
Temperature [K]	293(2)	293(2)	293(2)
Calculated density [g·cm^{-3}]	5.345	5.412	5.501
Crystal size [mm^3]	$0.07 \times 0.04 \times 0.03$	$0.08 \times 0.02 \times 0.02$	$0.06 \times 0.04 \times 0.02$
Detector distance [mm]	40.0	40.0	40.0
Exposure time per deg [sec]	215	105	180
Absorption coefficient [mm^{-1}]	20.60	21.90	23.43
$F(000)$	2064	2080	2096
θ Range [°]	3.0 to 32.5	3.0 to 37.5	3.0 to 32.0
Range in *hkl*	$-22/+24$, $-9/+11$, ± 18	± 27, ± 12, ± 20	± 23, ± 10, $-18/+17$
Scan type		φ/ω	
Total no. reflections	21671	37456	17570
Independent reflections	2793($R_{int} = 0.0962$)	4012($R_{int} = 0.0988$)	2637($R_{int} = 0.2056$)
Reflections with $I > 2\sigma(I)$	2397($R_\sigma = 0.0523$)	3524($R_\sigma = 0.0489$)	1568($R_\sigma = 0.1512$)
Data / parameters	2793 / 197	4012 / 197	2637 / 161
Absorption correction		numerical (HABITUS [52])	
Goodness-of-fit (F^2)	1.047	1.058	0.960
Final R indices [$I > 2\sigma(I)$]	$R1 = 0.0351$ $wR2 = 0.0628$	$R1 = 0.0294$ $wR2 = 0.0560$	$R1 = 0.0560$ $wR2 = 0.887$
R Indices (all data)	$R1 = 0.0470$ $wR2 = 0.0654$	$R1 = 0.0374$ $wR2 = 0.0580$	$R1 = 0.1284$ $wR2 = 0.1068$
Extinction coefficient	0.00031(5)	0.00061(5)	0.00007(5)
Larg. diff. peak a. hole [e·Å^{-3}]	2.38 / −2.32	2.85 / −4.80	3.28 / −3.27

of X-ray powder patterns and IR-spectra, they postulated the presence of three complementary structures subdivided into the groups REB_3O_6 (RE = Y, Ho, Er, Tm), REB_3O_6 (RE = Yb, Lu), and REB_3O_6 (RE = Dy). No further information about these higher homologues is available.

Using high-pressure/high-temperature conditions of 7.5 GPa and 1000 °C, we were able to synthesize the isotypic higher homologues of the orthorhombic phases $RE(BO_2)_3$ with RE = Dy–Lu from the starting materials RE_2O_3 and B_2O_3 in a 1:3 molar mixture without use of a flux or an excess of any of the components. We obtained the orthorhombic *meta*-oxoborates as single phase products for RE = Dy–Er. However, the compounds with RE = Tm–Lu were only obtained as byproducts of new high-pressure phases, which remained unidentified until now. Following to the pressure-homologue-rule [45], we were able to transform the structure of the lower homologues with smaller rare earth cations into that of their higher homologue $Tb(BO_2)_3$. A similar behaviour was observed for the normal pressure modification of α-CaB_4O_7, where the new high-pressure modification β-CaB_4O_7 is isotypic to the structure of its higher homologue SrB_4O_7 [46].

In this work, we report on the syntheses, crystal structures, and properties of the new orthorhombic rare earth *meta*-oxoborates $RE(BO_2)_3$ with RE = Dy–Lu.

Table 2. Crystal data and structure refinement for $RE(BO_2)_3$ (RE = Tm, Yb, Lu).

Empirical formula	TmB_3O_6	YbB_3O_6	LuB_3O_6
Molar mass [g·mol^{-1}]	297.36	301.47	303.40
Crystal system		orthorhombic	
Space group		*Pnma* (Nr. 62)	
Powder diffractometer		Stoe Stadi P	
Radiation		Cu-K$_{\alpha 1}$ ($\lambda = 154.06$ pm)	
Powder diffraction data			
a [pm]	1582.6(3)	1579.1(3)	1576.7(3)
b [pm]	736.8(3)	735.2(2)	734.9(2)
c [pm]	1216.4(3)	1214.0(3)	1211.7(3)
Volume [nm^3]	1.418(1)	1.410(1)	1.404(1)
Single crystal diffractometer		Enraf-Nonius Kappa CCD	
Radiation		Mo-K$_\alpha$ ($\lambda = 71.073$ pm)	
Single crystal data			
a [pm]	1581.6(2)		1576.7(2)
b [pm]	736.2(2)		734.7(2)
c [pm]	1216.2(2)		1211.5(2)
Volume [nm^3]	1.416(1)		1.403(1)
Formula units per cell		$Z = 16$	
Temperature [K]	293(2)		293(2)
Calculated density [g·cm^{-3}]	5.579		5.744
Crystal size [mm^3]	$0.07 \times 0.05 \times 0.02$		$0.05 \times 0.03 \times 0.02$
Detector distance [mm]	45.0		30.0
Exposure time per deg [sec]	60		350
Absorption coefficient [mm^{-1}]	24.99		28.06
$F(000)$	2112		2144
θ Range [°]	3.0 to 33.0		3.0 to 30.0
Range in *hkl*	−22/+24, −11/+10, −15/+18		±22, −9/+10, −16/+17
Scan type		φ/ω	
Total no. reflections	10413		32640
Independent reflections	2837($R_{int} = 0.1126$)		2192($R_{int} = 0.0974$)
Reflections with $I > 2\sigma(I)$	1888($R_\sigma = 0.1176$)		1794($R_\sigma = 0.0481$)
Data / parameters	2837 / 197		2192 / 197
Absorption correction		numerical (HABITUS [52])	
Goodness-of-fit (F^2)	0.905		1.057
Final R Indices [$I > 2\sigma(I)$]	$R1 = 0.0430$ $wR2 = 0.0720$		$R1 = 0.0282$ $wR2 = 0.0457$
R indices (all data)	$R1 = 0.0866$ $wR2 = 0.0812$		$R1 = 0.0439$ $wR2 = 0.0491$
Extinction coefficient	0.00102(7)		0.00030(3)
Larg. diff. peak a. hole [e·Å^{-3}]	3.24 / −3.59		1.89 / −1.99

Experimental Section

According to eq. (1), the starting materials for the syntheses of orthorhombic $RE(BO_2)_3$ (RE = Dy–Lu) were a 1:3 molar mixture of B_2O_3 [from H_3BO_3 (99.8%, Merck, Darmstadt) fired at 600 °C] with the rare earth oxides RE_2O_3 (RE= Dy–Lu; 99.9%).

$$RE_2O_3 + 3\,B_2O_3 \xrightarrow[1000\ ^\circ C]{7.5\,GPa} 2\,RE(BO_2)_3 (RE = \text{Dy–Lu}) \quad (1)$$

The starting materials were compressed and heated *via* multianvil assemblies. Details of the construction of the assemblies can be found in references [19] and [47 – 49]. For the syntheses of $RE(BO_2)_3$ (RE = Dy–Lu), the 18/11 assemblies were compressed within 3 h to 7.5 GPa and heated to 1000 °C in the following 8 min. After holding this temperature for 6 min, the samples were cooled down within another 10 min. After decompression, the recovered experimental octahedra were broken apart, and the samples carefully separated from the surrounding boron nitride. The compounds $RE(BO_2)_3$ (RE = Dy–Er) were obtained as single phase, crystalline products (yield: 75 mg per run). The substances are air- and humidity–resistant and crystallize as long, thin, colourless needles. The orthorhombic phases $RE(BO_2)_3$ of thulium, ytterbium, and lutetium were obtained as byproducts of new phases, which have not been characterized in detail until now. Compared to the orthorhombic phases, the part of the new unknown phases rises from the thulium to the lutetium compound.

Table 3. Atomic coordinates and isotropic equivalent displacement parameters U_{eq} [Å^2] for $Dy(BO_2)_3$ (space group *Pnma*). U_{eq} is defined as one third of the trace of the orthogonalized U_{ij} tensor.

Atom	Wyckoff-Position	*x*	*y*	*z*	U_{eq}
Dy1	4*c*	0.17179(3)	1/4	0.93356(3)	0.00667(9)
Dy2	4*c*	0.12063(3)	3/4	0.00762(3)	0.00660(9)
Dy3	4*c*	0.04828(3)	1/4	0.58840(3)	0.00689(9)
Dy4	4*c*	0.12747(3)	3/4	0.73076(3)	0.00668(9)
B1	8*d*	0.2823(4)	0.9295(9)	0.8146(5)	0.006(2)
B2	8*d*	0.9429(4)	0.9265(9)	0.6543(5)	0.006(2)
B3	8*d*	0.0313(5)	0.059(2)	0.8217(5)	0.010(2)
B4	8*d*	0.1534(4)	0.9228(9)	0.4824(5)	0.007(2)
B5	8*d*	0.1095(5)	0.0767(9)	0.1437(5)	0.009(2)
B6	8*d*	0.2577(4)	0.9329(9)	0.1285(5)	0.006(2)
O1	4*c*	0.1596(4)	3/4	0.5392(4)	0.006(2)
O2	8*d*	0.2818(3)	0.0632(5)	0.8987(3)	0.0071(8)
O3	8*d*	0.9307(3)	0.0585(5)	0.5683(3)	0.0053(7)
O4	8*d*	0.0483(3)	0.9351(6)	0.1229(3)	0.0069(8)
O5	8*d*	0.3709(3)	0.9263(6)	0.7655(3)	0.0069(8)
O6	8*d*	0.1848(3)	0.0340(6)	0.0775(3)	0.0073(8)
O7	4*c*	0.0636(4)	1/4	0.8024(4)	0.007(2)
O8	4*c*	0.2247(4)	3/4	0.1398(4)	0.009(2)
O9	8*d*	0.0965(3)	0.9604(6)	0.8776(3)	0.0076(8)
O10	8*d*	0.1643(3)	0.0654(6)	0.5644(3)	0.0059(7)
O11	4*c*	0.0774(4)	1/4	0.1065(4)	0.008(2)
O12	4*c*	0.2547(4)	3/4	0.8555(4)	0.008(2)
O13	4*c*	0.0491(4)	1/4	0.3969(4)	0.007(2)
O14	8*d*	0.0211(3)	0.9771(6)	0.7093(3)	0.0071(8)
O15	8*d*	0.2235(3)	0.9787(6)	0.7300(3)	0.0079(8)

Table 4. Atomic coordinates and isotropic equivalent displacement parameters U_{eq} [Å^2] for $Lu(BO_2)_3$ (space group *Pnma*). U_{eq} is defined as one third of the trace of the orthogonalized U_{ij} tensor.

Atom	Wyckoff-Position	*x*	*y*	*z*	U_{eq}
Lu1	4*c*	0.17332(2)	1/4	0.93655(3)	0.0083(2)
Lu2	4*c*	0.12124(2)	3/4	0.01004(3)	0.0086(2)
Lu3	4*c*	0.04861(2)	1/4	0.58923(3)	0.0087(2)
Lu4	4*c*	0.12806(2)	3/4	0.73580(3)	0.0081(2)
B1	8*d*	0.2821(4)	0.930(2)	0.8157(6)	0.010(2)
B2	8*d*	0.9439(4)	0.927(2)	0.6540(6)	0.007(2)
B3	8*d*	0.0334(4)	0.059(2)	0.8241(6)	0.008(2)
B4	8*d*	0.1512(4)	0.921(2)	0.4836(6)	0.009(2)
B5	8*d*	0.1101(4)	0.076(2)	0.1423(6)	0.009(2)
B6	8*d*	0.2587(4)	0.933(2)	0.1287(6)	0.008(2)
O1	4*c*	0.1568(4)	3/4	0.5445(5)	0.008(2)
O2	8*d*	0.2820(2)	0.0681(6)	0.8993(3)	0.007(2)
O3	8*d*	0.9322(3)	0.0622(6)	0.5693(4)	0.009(2)
O4	8*d*	0.0485(3)	0.9327(6)	0.1213(4)	0.009(2)
O5	8*d*	0.3713(3)	0.9265(6)	0.7655(3)	0.007(2)
O6	8*d*	0.1860(2)	0.0357(6)	0.0758(3)	0.008(2)
O7	4*c*	0.0675(4)	1/4	0.8047(5)	0.011(2)
O8	4*c*	0.2242(4)	3/4	0.1400(5)	0.008(2)
O9	8*d*	0.0973(3)	0.9551(6)	0.8807(4)	0.010(1)
O10	8*d*	0.1626(3)	0.0682(6)	0.5641(3)	0.008(1)
O11	4*c*	0.0774(4)	1/4	0.1036(5)	0.009(2)
O12	4*c*	0.2543(4)	3/4	0.8598(5)	0.008(2)
O13	4*c*	0.0475(4)	1/4	0.3998(5)	0.008(2)
O14	8*d*	0.0238(3)	0.9733(6)	0.7111(4)	0.008(2)
O15	8*d*	0.2221(3)	0.9763(6)	0.7309(3)	0.008(1)

Crystal Structure Analysis

The powder diffraction data of the orthorhombic $RE(BO_2)_3$ (*RE* = Dy–Lu) compounds were collected on a STOE Stadi P diffractometer with monochromatized Cu-$K_{\alpha 1}$ radiation. The diffraction patterns were indexed with the program ITO [50] on the basis of an orthorhombic unit cell. The lattice parameters (Table 1 and 2) were obtained from least–squares fits of the powder data. The correct indexing of the patterns was confirmed by intensity calculations [51], taking the atomic positions from the structure refinements for $RE(BO_2)_3$ (*RE* = Dy–Er, Lu). The lattice parameters, determined from powders and single crystals, tally well. For indexing of the orthorhombic phases $RE(BO_2)_3$ (*RE* = Tm–Lu), found as byproducts, only corresponding reflections were used.

Small single crystals of $RE(BO_2)_3$ (*RE* = Dy–Tm, Lu) were isolated by mechanical fragmentation and examined by Buerger precession photographs. Single crystal intensity data were collected from regularly shaped colorless crystals (rods) at room temperature by use of an Enraf-Nonius Kappa CCD, equipped with a rotating anode [Mo-K_α radiation (71.073 pm)]. A numerical absorption correction (HABITUS [52]) was applied to all data. All relevant information concerning the data collections is listed in Tables 1 and 2. According to the systematic extinctions $0kl$ with $k + l \neq 2n$ and $hk0$ with $h \neq 2n$, the space groups $Pn2_1a$ (No. 33) and *Pnma* (No. 62) were derived. The centrosymmetric group was found to be correct during the structure refinement. The starting positional parameters were deduced from an automatic interpretation of direct methods with SHELXS-97 [53]. The structures of $RE(BO_2)_3$ (*RE* = Dy, Ho, Tm, Lu) were successfully refined with anisotropic displacement parameters for all atoms with SHELXL-97 [54] (full-matrix least-squares on F^2). The structures of $RE(BO_2)_3$ (*RE* = Er) could only partially be refined with anisotropic displacement parameters due to the low quality of the single crystals obtained. Final difference Fourier syntheses revealed no significant residual peaks in all refinements (see Tables 1 and 2). The parameters for the single–crystal structure mea-

Table 5. Anisotropic displacement parameters [Å^2] for $Dy(BO_2)_3$ (space group *Pnma*).

Atom	U_{11}	U_{22}	U_{33}	U_{12}	U_{13}	U_{23}
Dy1	0.0098(2)	0.0057(2)	0.0045(2)	0	−0.0000(2)	0
Dy2	0.0112(2)	0.0052(2)	0.0034(2)	0	−0.0002(2)	0
Dy3	0.0095(2)	0.0062(2)	0.0049(2)	0	0.0000(2)	0
Dy4	0.0098(2)	0.0059(2)	0.0043(2)	0	0.0002(2)	0
B1	0.003(3)	0.007(3)	0.009(2)	0.001(2)	0.001(2)	0.002(2)
B2	0.006(3)	0.007(3)	0.004(2)	0.000(2)	0.000(2)	0.000(2)
B3	0.013(3)	0.013(3)	0.005(2)	−0.002(3)	0.001(2)	0.001(2)
B4	0.012(3)	0.005(3)	0.004(2)	−0.003(2)	−0.001(2)	0.001(2)
B5	0.015(3)	0.006(3)	0.006(2)	0.001(2)	−0.001(2)	−0.003(2)
B6	0.010(3)	0.006(3)	0.003(2)	−0.003(2)	0.000(2)	0.000(2)
O1	0.009(3)	0.004(3)	0.006(2)	0	0.000(2)	0
O2	0.013(2)	0.003(2)	0.006(2)	−0.000(2)	−0.002(2)	−0.001(2)
O3	0.005(2)	0.005(2)	0.006(2)	0.001(2)	−0.002(2)	0.000(2)
O4	0.009(2)	0.007(2)	0.005(2)	−0.002(2)	−0.000(2)	−0.000(2)
O5	0.007(2)	0.011(2)	0.003(2)	−0.001(2)	0.000(2)	−0.003(2)
O6	0.011(2)	0.008(2)	0.002(2)	0.000(2)	0.001(2)	−0.002(2)
O7	0.006(3)	0.008(3)	0.008(2)	0	−0.001(2)	0
O8	0.011(3)	0.006(3)	0.010(3)	0	0.000(2)	0
O9	0.009(2)	0.010(2)	0.004(2)	0.002(2)	0.002(2)	0.001(2)
O10	0.005(2)	0.007(2)	0.006(2)	0.004(2)	−0.002(2)	−0.001(2)
O11	0.014(3)	0.006(3)	0.003(2)	0	−0.001(2)	0
O12	0.012(3)	0.008(3)	0.003(2)	0	0.002(2)	0
O13	0.012(3)	0.005(3)	0.003(2)	0	0.002(2)	0
O14	0.009(2)	0.010(2)	0.003(2)	0.001(2)	−0.000(2)	−0.002(2)
O15	0.010(2)	0.011(2)	0.003(2)	0.001(2)	−0.001(2)	0.000(2)

Table 6. Anisotropic displacement parameters [Å^2] for $Lu(BO_2)_3$ (space group *Pnma*).

Atom	U_{11}	U_{22}	U_{33}	U_{12}	U_{13}	U_{23}
Lu1	0.0081(2)	0.0084(2)	0.0084(2)	0	0.0002(1)	0
Lu2	0.0101(2)	0.0080(2)	0.0076(2)	0	0.0000(2)	0
Lu3	0.0077(2)	0.0092(2)	0.0092(2)	0	0.0000(2)	0
Lu4	0.0082(2)	0.0079(2)	0.0081(2)	0	0.0001(2)	0
B1	0.009(3)	0.010(4)	0.010(4)	0.001(3)	−0.001(3)	−0.002(3)
B2	0.007(3)	0.008(3)	0.005(3)	−0.002(3)	0.003(3)	0.001(3)
B3	0.009(3)	0.009(4)	0.007(4)	−0.002(3)	0.001(3)	−0.002(3)
B4	0.007(3)	0.011(4)	0.009(4)	0.004(3)	−0.001(3)	0.002(3)
B5	0.007(3)	0.010(4)	0.009(4)	−0.003(3)	0.002(3)	−0.005(3)
B6	0.009(3)	0.006(4)	0.009(4)	0.001(3)	−0.004(3)	0.001(3)
O1	0.005(3)	0.008(3)	0.011(3)	0	−0.002(2)	0
O2	0.004(2)	0.012(2)	0.006(2)	−0.002(2)	−0.003(2)	0.000(2)
O3	0.008(2)	0.010(2)	0.008(2)	0.003(2)	0.000(2)	0.000(2)
O4	0.011(2)	0.006(2)	0.008(2)	−0.001(2)	−0.003(2)	−0.002(2)
O5	0.008(2)	0.009(2)	0.005(2)	0.001(2)	0.001(2)	0.000(2)
O6	0.005(2)	0.010(2)	0.008(2)	0.002(2)	−0.001(2)	−0.001(2)
O7	0.006(3)	0.008(3)	0.018(4)	0	0.007(3)	0
O8	0.009(3)	0.009(3)	0.007(3)	0	0.003(2)	0
O9	0.009(2)	0.007(2)	0.014(2)	0.001(2)	−0.003(2)	0.002(2)
O10	0.010(2)	0.008(2)	0.006(2)	0.001(2)	−0.001(2)	0.001(2)
O11	0.007(3)	0.010(3)	0.011(3)	0	−0.003(3)	0
O12	0.009(3)	0.010(3)	0.005(3)	0	0.002(2)	0
O13	0.005(3)	0.008(3)	0.010(3)	0	0.002(2)	0
O14	0.008(2)	0.011(2)	0.005(2)	−0.001(2)	0.000(2)	−0.003(2)
O15	0.008(2)	0.011(2)	0.005(2)	0.000(2)	0.000(2)	0.000(2)

surements are listed in Tables 1 and 2. The compounds are isotypic, therefore the positional parameters (Table 3 and 4), anisotropic displacement parameters (Table 5 and 6), interatomic distances (Table 7, 8, 9, 10, and 11), and angles (Table 12 and 13) were listed only for the component with the largest rare earth cation ($Dy(BO_2)_3$) and with the smallest rare earth cation ($Lu(BO_2)_3$) of the presented series. Further details of the crystal structure investigations for all compounds may be obtained from the Fachinforma-

B1–O2	142.8(7)	B2–O3	145.1(7)	B3–O4	143.9(8)	B4–O1	146.0(7)
B1–O5	153.5(8)	B2–O5	151.1(7)	B3–O7	152.3(7)	B4–O2	146.0(8)
B1–O12	148.7(7)	B2–O13	145.5(7)	B3–O9	144.3(8)	B4–O3	148.3(8)
B1–O15	144.3(7)	B2–O14	146.6(8)	B3–O14	151.4(7)	B4–O10	146.8(7)
	⌀ 147.3		⌀ 147.1		⌀ 148.0		⌀ 146.8
B5–O4	145.4(8)	B6–O6	151.7(8)				
B5–O5	152.7(7)	B6–O8	145.9(7)				
B5–O6	148.2(8)	B6–O10	147.0(8)				
B5–O11	145.4(7)	B6–O15	143.9(7)				
	⌀ 147.9		⌀ 147.1		⌀ over all distances 147.4		

Table 7. Interatomic B–O distances [pm] calculated with the single crystal lattice parameters in $Dy(BO_2)_3$ (Standard deviations in parentheses).

B1–O2	143.3(9)	B2–O3	144.1(8)	B3–O4	145.3(8)	B4–O1	146.2(8)
B1–O5	153.2(8)	B2–O5	150.4(8)	B3–O7	152.2(8)	B4–O2	146.9(8)
B1–O12	149.2(8)	B2–O13	146.0(8)	B3–O9	143.7(8)	B4–O3	146.9(8)
B1–O15	143.8(8)	B2–O14	147.8(8)	B3–O14	151.4(8)	B4–O10	146.5(9)
	⌀ 147.4		⌀ 147.1		⌀ 148.1		⌀ 146.6
B5–O4	145.5(8)	B6–O6	151.6(8)				
B5–O5	152.1(9)	B6–O8	145.5(8)				
B5–O6	147.2(8)	B6–O10	146.7(8)				
B5–O11	145.6(8)	B6–O15	144.0(9)				
	⌀ 147.6		⌀ 147.0		⌀ over all distances 147.3		

Table 8. Interatomic B–O distances [pm] calculated with the single crystal lattice parameters in $Lu(BO_2)_3$ (Standard deviations in parentheses).

Dy1–O2a	227.3(4)	Dy2–O9a	226.2(4)	Dy3–O10a	231.7(4)	Dy4–O15a	228.2(4)
Dy1–O2b	227.3(4)	Dy2–O9b	226.2(4)	Dy3–O10b	231.7(4)	Dy4–O15b	228.2(4)
Dy1–O7	235.7(6)	Dy2–O4a	228.2(4)	Dy3–O13	234.9(5)	Dy4–O14a	240.1(4)
Dy1–O6a	239.1(4)	Dy2–O4b	228.2(4)	Dy3–O3a	236.2(4)	Dy4–O14b	240.1(4)
Dy1–O6b	239.1(4)	Dy2–O8	231.9(6)	Dy3–O3b	236.2(4)	Dy4–O1	240.4(5)
Dy1–O9a	255.1(4)	Dy2–O6a	249.0(4)	Dy3–O14a	254.3(4)	Dy4–O9a	243.1(4)
Dy1–O9b	255.1(4)	Dy2–O6b	249.0(4)	Dy3–O14b	254.3(4)	Dy4–O9b	243.1(4)
Dy1–O11	260.0(6)	Dy2–O12	283.6(6)	Dy3–O7	263.6(5)	Dy4–O12	253.9(6)
	⌀ 242.3		⌀ 240.3		⌀ 242.8		⌀ 239.6
			⌀ over all distances 241.3				

Table 9. Interatomic Dy–O distances [pm] calculated with the single crystal lattice parameters in $Dy(BO_2)_3$ (Standard deviations in parentheses).

Lu1–O2a	222.0(4)	Lu2–O9a	220.7(4)	Lu3–O10a	225.9(4)	Lu4–O15a	222.8(4)
Lu1–O2b	222.0(4)	Lu2–O9b	220.7(4)	Lu3–O10b	225.9(4)	Lu4–O15b	222.8(4)
Lu1–O7	230.9(6)	Lu2–O4a	222.1(4)	Lu3–O13	229.5(6)	Lu4–O14a	234.1(4)
Lu1–O6a	231.6(4)	Lu2–O4b	222.1(4)	Lu3–O3a	230.8(4)	Lu4–O14b	234.1(4)
Lu1–O6b	231.6(4)	Lu2–O8	226.1(6)	Lu3–O3b	230.8(4)	Lu4–O1	236.2(6)
Lu1–O11	252.6(6)	Lu2–O6a	246.6(4)	Lu3–O14a	254.2(4)	Lu4–O9a	236.4(5)
Lu1–O9a	256.7(4)	Lu2–O6b	246.6(4)	Lu3–O14b	254.2(4)	Lu4–O9b	236.4(5)
Lu1–O9b	256.7(4)	Lu2–O12	277.8(6)	Lu3–O7	262.8(7)	Lu4–O12	249.3(6)
	⌀ 238.0		⌀ 235.3		⌀ 239.3		⌀ 234.0
			⌀ over all distances 236.7				

Table 10. Interatomic Lu–O distances [pm] calculated with the single crystal lattice parameters in $Lu(BO_2)_3$ (Standard deviations in parentheses).

tionszentrum Karlsruhe, 76344 Eggenstein Leopoldshafen, Germany (fax: (+49)7247-808-666; e-mail: crysdata@fiz-karlsruhe.de), on quoting the depository number CSD-413582 for $Dy(BO_2)_3$, CSD-413584 for $Ho(BO_2)_3$, CSD-413583 for $Er(BO_2)_3$, CSD-413586 for $Tm(BO_2)_3$, and CSD-413585 for $Lu(BO_2)_3$.

Results and Discussion

The crystal structures of orthorhombic $RE(BO_2)_3$ (RE = Dy–Lu) compounds contain strongly corrugated oxoborate layers, built up of corner-sharing BO_4-tetrahedra, which spread out perpendicular to [100] (Fig. 1). The Fundamental Building Block (FBB) of the B–O-structure is built up around two three-coordinate oxygen atoms O[3], which represent a rare feature of bridging of BO_4-tetrahedra in oxoborate chemistry. Figure 2a gives a view of the FBB approximately along [010], and Fig. 2b along [100]. Precisely, starting from a three-coordinate oxygen atom

Table 11. Comparison of the O(5)–B distances [pm] in $RE(BO_2)_3$ (RE = Dy–Tm, Lu).

	$Dy(BO_2)_3$	$Ho(BO_2)_3$	$Er(BO_2)_3$	$Tm(BO_2)_3$	$Lu(BO_2)_3$
O5–B2	151.1(7)	150.8(4)	151(2)	153(2)	150.4(8)
O5–B5	152.7(7)	153.4(4)	154(2)	154(2)	152.1(9)
O5–B1	153.5(8)	153.8(4)	153(2)	151(2)	153.2(8)
	⌀ 152.4	⌀ 152.7	⌀ 152.7	⌀ 152.7	⌀ 151.9

Table 12. Interatomic angles [°] calculated with the single crystal lattice parameters in $Dy(BO_2)_3$ (Standard deviations in parentheses).

O2–B1–O15	109.9(5)	O3–B2–O13	107.6(4)	O4–B3–O9	115.2(5)
O2–B1–O12	112.0(5)	O3–B2–O14	106.0(5)	O4–B3–O14	110.3(5)
O15–B1–O12	106.0(5)	O13–B2–O14	110.7(5)	O9–B3–O14	107.9(5)
O2–B1–O5	107.4(5)	O3–B2–O5	111.8(5)	O4–B3–O7	110.0(5)
O15–B1–O5	108.5(4)	O13–B2–O5	110.3(5)	O9–B3–O7	107.5(5)
O12–B1–O5	113.0(5)	O14–B2–O5	110.3(4)	O14–B3–O7	105.5(5)
	⌀ 109.5		⌀ 109.5		⌀ 109.4
O1–B4–O2	110.5(5)	O11–B5–O4	110.2(5)	O15–B6–O8	114.5(5)
O1–B4–O10	107.2(4)	O11–B5–O6	107.5(5)	O15–B6–O10	106.4(5)
O2–B4–O10	110.3(5)	O4–B5–O6	107.0(5)	O8–B6–O10	111.3(5)
O1–B4–O3	110.1(5)	O11–B5–O5	113.1(5)	O15–B6–O6	106.9(5)
O2–B4–O3	109.7(4)	O4–B5–O5	107.4(5)	O8–B6–O6	102.8(5)
O10–B4–O3	109.1(5)	O6–B5–O5	111.5(5)	O10–B6–O6	115.0(4)
	⌀ 109.5		⌀ 109.5		⌀ 109.5
		⌀ over all angles 109.5			

Table 13. Interatomic angles [°] calculated with the single crystal lattice parameters in $Lu(BO_2)_3$ (Standard deviations in parentheses).

O2–B1–O15	109.6(5)	O3–B2–O13	107.9(5)	O4–B3–O9	115.4(6)
O2–B1–O12	112.0(6)	O3–B2–O14	106.4(5)	O4–B3–O14	109.9(5)
O15–B1–O12	105.8(5)	O13–B2–O14	109.6(5)	O9–B3–O14	106.3(5)
O2–B1–O5	107.0(5)	O3–B2–O5	111.5(5)	O4–B3–O7	110.2(5)
O15–B1–O5	108.9(5)	O13–B2–O5	111.0(5)	O9–B3–O7	108.4(5)
O12–B1–O5	113.4(5)	O14–B2–O5	110.3(5)	O14–B3–O7	106.2(5)
	⌀ 109.5		⌀ 109.5		⌀ 109.4
O1–B4–O2	110.7(5)	O11–B5–O4	110.1(5)	O15–B6–O8	115.2(6)
O1–B4–O10	106.9(5)	O11–B5–O6	106.7(6)	O15–B6–O10	106.4(5)
O2–B4–O10	109.7(5)	O4–B5–O6	107.5(5)	O8–B6–O10	111.3(5)
O1–B4–O3	110.2(6)	O11–B5–O5	113.2(6)	O15–B6–O6	106.9(5)
O2–B4–O3	109.5(5)	O4–B5–O5	106.9(5)	O8–B6–O6	102.5(5)
O10–B4–O3	109.9(5)	O6–B5–O5	112.2(5)	O10–B6–O6	114.6(5)
	⌀ 109.5		⌀ 109.4		⌀ 109.5
		⌀ over all angles 109.5			

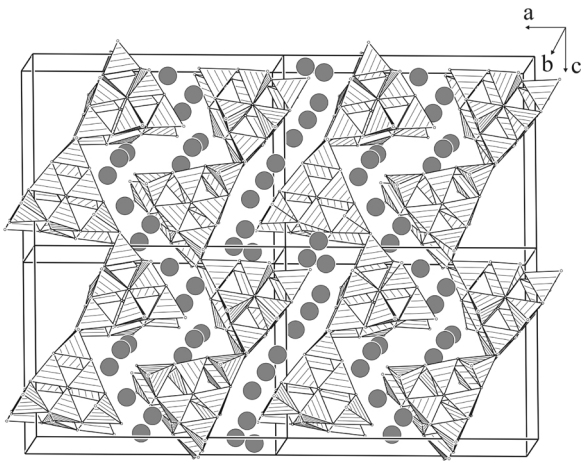

Fig. 1. Crystal structure of the orthorhombic $RE(BO_2)_3$ compounds (RE = Dy–Lu).

$O^{[3]}$, three BO_4-tetrahedra are linked together at this atom. At a time, two of these BO_4-tetrahedra build up a three-membered ring, each with an additional BO_4-tetrahedron, such that the three built up three-membered rings form a nearly equilateral triangle. These triangles are linked on one side *via* three remaining corners of the inner three BO_4-tetrahedra, and on the other side *via* the free corners of the outer BO_4-tetrahedra (Fig. 3). The FBB-piles are linked to corrugated layers *via* the O(10)-atoms on two further corners of the triangles. To examine the ring sizes in the structure topologically, we calculated the cycle class sequences for $RE(BO_2)_3$ (RE = Dy–Tm, Lu), speci-

Table 14. Cycle-class sequences of $RE(BO_2)_3$ (RE = Dy–Tm, Lu) [55 – 58].

Ring Size n	3	4	5	6	7	8	9	10	11
$RE(BO_2)_3$	24	12	48	96	176	252	368	908	1928

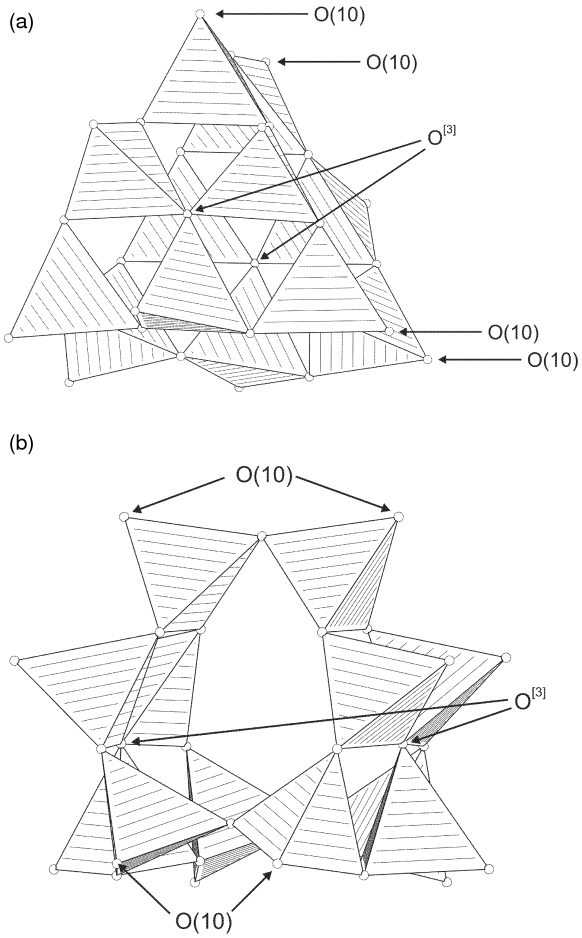

Fig. 2. Fundamental Building Block of $RE(BO_2)_3$ (RE = Dy–Lu), view approximately along (a) [010], (b) [100].

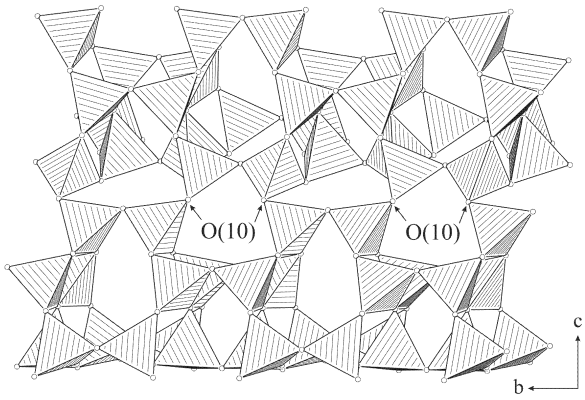

Fig. 3. Linkage of the Fundamental Building Blocks in $RE(BO_2)_3$ (RE = Dy–Lu) along [010].

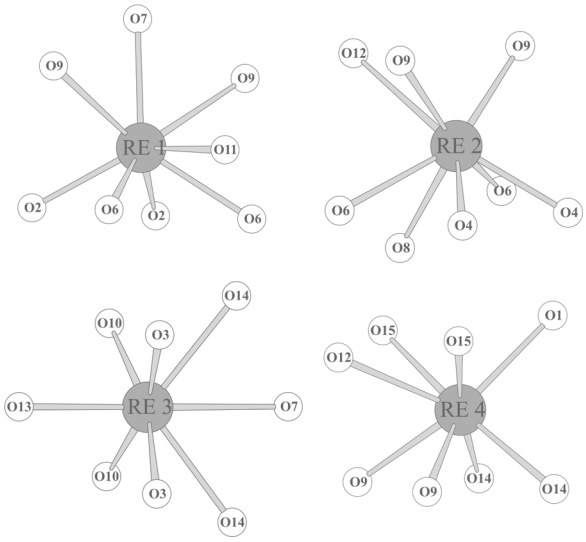

Fig. 4. Coordination spheres of RE^{3+} (gray spheres) in the crystal structure of $RE(BO_2)_3$ (RE = Dy–Lu).

fying the relative abundance of B_nO_n ring sizes (for $n = 3-11$) per unit cell [55–58]. The results are given in Table 14.

The RE^{3+} (RE^{3+} = Dy^{3+}–Lu^{3+}) ions are positioned between the layers. Each of the four crystallographically different RE^{3+} cations is coordinated by eight oxygen atoms (Fig. 4). In the case of RE^{3+} = Dy^{3+}, the bond-lengths in the coordination polyhedra vary between 226 and 284 pm (Table 9). For $Ho(BO_2)_3$, $Er(BO_2)_3$, $Tm(BO_2)_3$, and $Lu(BO_2)_3$ (Table 10) the bond-lengths lie in the range 226–282, 226–282, 222–282, and 221–278 pm, respectively.

The B–O bond-lengths in $RE(BO_2)_3$ (RE = Dy–Tm, Lu) vary between 143–154 ($Dy(BO_2)_3$), 144–154 ($Ho(BO_2)_3$), 140–155 ($Er(BO_2)_3$), 143–155 ($Tm(BO_2)_3$), and 143–153 pm ($Lu(BO_2)_3$). The average B–O bond-length of each compound with the values 147.4 (RE = Dy) (Table 7), 147.5 (RE = Ho), 147.5 (RE = Er), 147.2 (RE = Tm), and 147.3 pm (RE = Lu) (Table 8) correspond to the known average value of 147.6 pm for oxoborates [59]. The O–B–O angles in the BO_4-tetrahedra vary between 102.8–115.2° for $Dy(BO_2)_3$, 102.7–114.8° for $Ho(BO_2)_3$, 100.8–116.1° for $Er(BO_2)_3$, 102.3–116.1° for $Tm(BO_2)_3$, and 102.5–115.4° for $Lu(BO_2)_3$. The B–O bond-lengths in the OB_3-groups around the three-coordinate O(5)-atoms of the compounds vary between 151–154 pm for $RE(BO_2)_3$ with RE = Dy–Tm, and 150–153 pm for $Lu(BO_2)_3$ (Table 11). According to the linkage of the FBBs along [010] in all isotypic compounds (Fig. 3), the decrease of the lattice parameter b is much lower than the decrease in the other two axes. This is caused by the contraction along *a* and *c*, but not *b*, in accordance with the shrinking radius of the RE^{3+} cations due to the lanthanoid contraction (Table 15 and Fig. 5).

For further clarification, we calculated bond-valence sums for $RE(BO_2)_3$ (RE = Dy–Tm, Lu) with the bond-length/bond-strength and CHARDI concept (Table 16) [60–62]. The formal ionic charges of the atoms, acquired by the X-ray structure analysis,

Table 15. Comparison of the lattice parameters [pm] and volumes [nm^3] of $RE(BO_2)_3$ (RE = Tb–Lu).

Compound	*a*	*b*	*c*	*V*
$Tb(BO_2)_3$ [33]	1598.97(9)	741.39(4)	1229.58(7)	1.458
$Dy(BO_2)_3$	1592.4(1)	739.7(1)	1225.0(1)	1.443(1)
$Ho(BO_2)_3$	1590.0(4)	739.3(2)	1223.1(4)	1.438(1)
$Er(BO_2)_3$	1589.1(2)	737.6(1)	1219.1(1)	1.429(1)
$Tm(BO_2)_3$	1582.6(3)	736.8(3)	1216.4(3)	1.418(1)
$Yb(BO_2)_3$	1579.1(3)	735.2(2)	1214.0(3)	1.410(1)
$Lu(BO_2)_3$	1576.7(3)	734.9(2)	1211.7(3)	1.404(1)

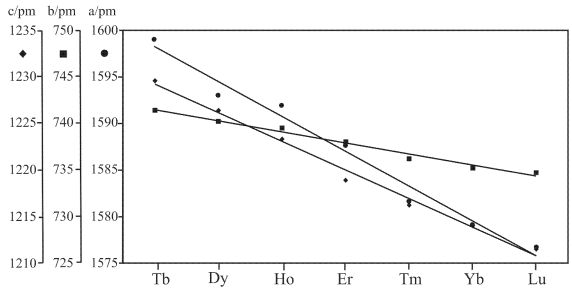

Fig. 5. Plot of the lattice parameters of the rare-earth *meta*-oxoborates $RE(BO_2)_3$ (RE = Tb–Lu).

Table 16. Charge distribution in $RE(BO_2)_3$ (RE = Dy–Tm, Lu) calculated with the bond-length / bond-strength concept (ΣV) [60,61] and the CHARDI concept (ΣQ) [62].

	ΣV	ΣQ		ΣV	ΣQ		ΣV	ΣQ		ΣV	ΣQ		ΣV	ΣQ
Dy1	+2.96	+2.97	Ho1	+2.94	+2.97	Er1	+2.93	+3.01	Tm1	+2.90	+3.02	Lu1	+2.83	+3.05
Dy2	+3.28	+2.94	Ho2	+3.24	+2.93	Er2	+3.26	+2.98	Tm2	+3.24	+2.88	Lu2	+3.17	+2.92
Dy3	+2.90	+3.03	Ho3	+2.85	+3.01	Er3	+2.86	+2.96	Tm3	+2.85	+3.00	Lu3	+2.53	+2.98
Dy4	+3.09	+2.98	Ho4	+3.06	+2.98	Er4	+3.08	+2.97	Tm4	+3.09	+2.98	Lu4	+3.00	+2.99
B1	+3.05	+3.04		+3.03	+3.06		+3.05	+3.06		+3.11	+3.10		+3.05	+3.06
B2	+3.06	+3.06		+3.04	+3.06		+3.04	+3.10		+3.03	+3.01		+3.06	+3.02
B3	+3.00	+2.98		+2.98	+2.98		+3.00	+3.00		+2.99	+2.99		+2.98	+3.02
B4	+3.08	+2.98		+3.09	+3.00		+3.02	+2.95		+3.10	+3.01		+3.09	+2.97
B5	+2.99	+3.06		+2.99	+3.05		+2.99	+3.05		+3.03	+3.05		+3.02	+3.05
B6	+3.06	+2.93		+3.06	+2.91		+3.11	+2.88		+3.09	+2.89		+3.07	+2.90
O1	−1.94	−1.94		−1.93	−1.89		−1.94	−1.95		−1.90	−1.83		−1.91	−1.88
O2	−2.17	−2.19		−2.12	−2.14		−2.07	−2.07		−2.17	−2.18		−2.12	−2.15
O3	−1.96	−1.97		−1.99	−2.01		−1.96	−2.00		−1.97	−1.98		−2.00	−2.05
O4	−2.15	−2.19		−2.12	−2.17		−2.11	−2.14		−2.17	−2.23		−2.11	−2.20
O5	−1.98	−1.80		−1.97	−1.80		−1.96	−1.76		−1.98	−1.76		−2.01	−1.83
O6	−2.09	−2.01		−2.08	−2.01		−2.05	−1.94		−2.08	−1.98		−2.09	−2.02
O7	−1.94	−1.85		−1.96	−1.91		−1.98	−1.93		−1.82	−1.68		−1.90	−1.68
O8	−2.04	−2.02		−2.07	−2.06		−2.01	−1.96		−2.12	−2.11		−2.05	−2.04
O9	−1.96	−1.96		−1.95	−1.97		−1.96	−1.97		−1.98	−2.01		−1.91	−1.97
O10	−2.00	−1.98		−1.98	−1.97		−2.07	−2.12		−2.01	−1.99		−2.00	−2.02
O11	−1.82	−1.86		−1.83	−1.88		−1.91	−2.01		−1.84	−1.87		−1.81	−1.83
O12	−1.84	−1.70		−1.82	−1.70		−1.86	−1.75		−1.80	−1.61		−1.80	−1.65
O13	−2.02	−2.04		−2.00	−2.03		−1.99	−2.03		−2.06	−2.13		−1.99	−2.04
O14	−2.08	−2.03		−2.05	−2.01		−2.01	−1.94		−2.08	−2.06		−2.01	−2.01
O15	−2.19	−2.18		−2.16	−2.19		−2.24	−2.26		−2.19	−2.19		−2.16	−2.19

are in agreement within the limits of the concepts. Additionally, we calculated MAPLE values (**Ma**delung **P**art of **L**attice **E**nergy) [63 – 65] for $RE(BO_2)_3$ (RE = Dy–Tm, Lu) to compare them with MAPLE values from the binary components RE_2O_3 (RE = Dy–Tm, Lu) and the high-pressure modification B_2O_3–II [1/2·RE_2O_3 (RE = Dy (15247 kJ mol^{-1}), Ho (15275 kJ mol^{-1}), Er (15350 kJ mol^{-1}), Tm (15517 kJ mol^{-1}), Lu (15589 kJ mol^{-1})) + 1½·B_2O_3–II (21938 kJ mol^{-1})] [66]. The deviation of the calculated values are in the range between 0.03 and 0.13% (Table 17).

Table 17. MAPLE values [kJ·mol^{-1}] of $RE(BO_2)_3$ (RE = Dy–Tm, Lu) in comparison with the MAPLE values [kJ·mol^{-1}] of the binary oxides RE_2O_3 (RE = Dy–Tm, Lu) and the high-pressure modification B_2O_3-II, and their deviation [%].

Compound	calculated MAPLE	MAPLE from binary oxides	Deviation
$Dy(BO_2)_3$	40581	40530	0.13
$Ho(BO_2)_3$	40577	40544	0.08
$Er(BO_2)_3$	40610	40582	0.07
$Tm(BO_2)_3$	40680	40665	0.04
$Lu(BO_2)_3$	40712	40701	0.03

In-situ powder diffraction and thermoanalytical measurements

To investigate the high–temperature behaviour of the new phases $RE(BO_2)_3$ (RE = Dy–Er), temperature dependent *in-situ* X-ray diffractometry was performed on a STOE powder diffractometer Stadi P (Mo-K_α; $\lambda = 71.073$ pm) with a computer-controlled STOE furnace. An electrically heated graphite tube held the sample capillary vertical with respect to the scattering plane. Bores in the graphite tube permitted unobstructed pathways for the primary beam as well as for the scattered radiation. The temperature measured by a thermocouple in the graphite tube was kept constant within 0.2 °C. The heating rate between different temperatures was set to 22 °C/min. For temperature stabilization, a time of three minutes was allowed before starting each data acquisition. Successive heating of the phases $RE(BO_2)_3$ (RE = Dy, Ho) in the range of 900 – 1000 °C lead to decomposition into the high-temperature modification μ-$DyBO_3$ [5] and molten B_2O_3 for $Dy(BO_2)_3$. $Ho(BO_2)_3$ decomposes at approximately 900 °C into the high-temperature modification μ-$HoBO_3$, the room temperature modification π-$HoBO_3$, and molten B_2O_3. Fig. 6 shows the results for orthorhombic $Dy(BO_2)_3$ (top) and $Ho(BO_2)_3$ (below). Subsequent cooling leads to complete transformation into room temperature modifications π-$REBO_3$

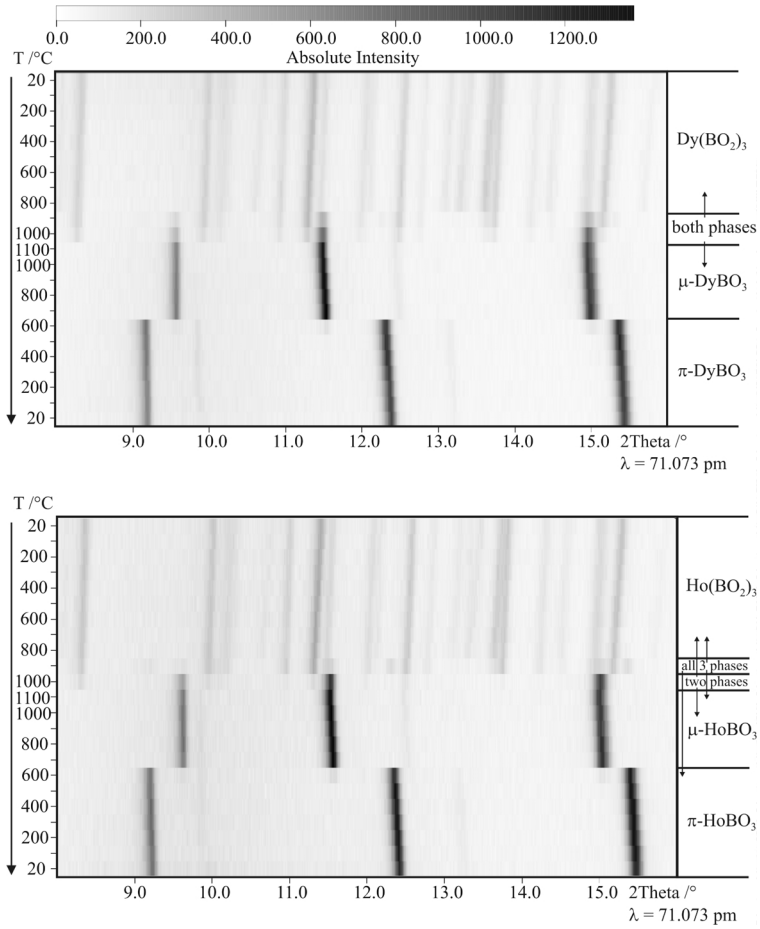

Fig. 6. Temperature-dependent X-ray powder patterns following the decomposition reaction of $Dy(BO_2)_3$ (top) and $Ho(BO_2)_3$ (below).

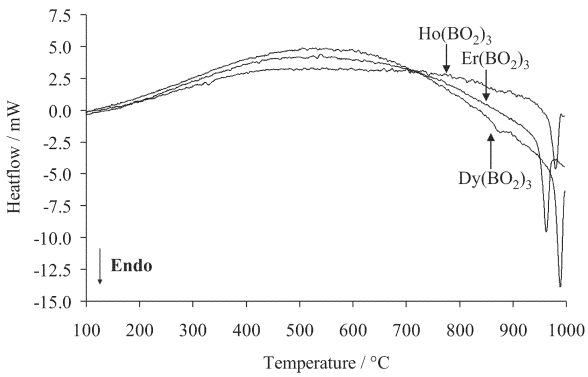

Fig. 7. Differential thermal analysis curves of $RE(BO_2)_3$ (RE = Dy–Er).

(RE = Dy, Ho) at 600 °C. These results were confirmed by thermoanalytical measurements, which were performed with a combined DTA-TG-thermobalance (TGA 92-2400, Setaram, heating rate: 10 °C min^{-1}) between room temperature and 1000 °C. While heating, broad endothermic effects occur in the DTA between 970–1000 °C for $Dy(BO_2)_3$, 960–990 °C for $Ho(BO_2)_3$, and 940–980 °C for $Er(BO_2)_3$ (Fig. 7), due to the decomposition of the compounds into the high-temperature modifications μ-REBO$_3$ (RE = Dy–Er) and molten B_2O_3.

Infrared spectroscopy

The infrared (IR) spectra of $RE(BO_2)_3$ (RE = Dy, Ho, Er) were recorded on a Bruker IFS66/v spectrometer scanning a range from 400 to 4000 cm^{-1}. The samples were thoroughly mixed with dried KBr (5 mg sample, 500 mg KBr) in a glove box under dried argon atmosphere. Fig. 8 shows the section 400–2000 cm^{-1} of the infrared spectra of the dysprosium, erbium and thulium compound. The absorption peaks between 790 and 1150 cm^{-1} are those typical for the

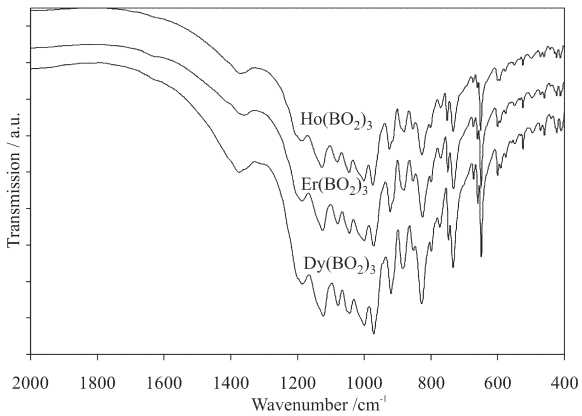

Fig. 8. IR spectra of $RE(BO_2)_3$ (RE = Dy–Er).

tetrahedral borate group BO_4 as in YBO_3, $GdBO_3$, or $TaBO_4$ [67–69]. Between 1300 and 1400 cm^{-1}, around 1200 cm^{-1}, and below 790 cm^{-1}, we observe absorptions, which are normally typical for triangular BO_3-groups as in $LaBO_3$ [70, 71] or EuB_2O_4 [72]. Since BO_3-groups are absent in the investigated compounds, the absorptions could be assigned to the corresponding OB_3-vibrations. Analogous geometrics and similar force parameters in the OB_3-group recommend this assignment, as it is valid also for β-ZnB_4O_7 [73], β-CaB_4O_7 [46], and $Na_3[B_6O_9(VO_4)]$ [74]. Additionally, the absorption spectra reported by Weir *et al.* [75] for SrB_4O_7 [76] and PbB_4O_7 [77], which also exhibit OB_3-groups next to BO_4-groups, show similar absorption bands as $RE(BO_2)_3$ (RE = Dy, Ho, Er). The existence of six crystallographically independent BO_4-units in the structure of $Dy(BO_2)_3$, in combination with OB_3-groups, render a detailed assignment of the broad bands more difficult. In the upper range (4000–2000 cm^{-1}) no absorption bands due to hydrogen (OH) could be found. A comparison of our IR-spectra to those obtained by Tananaev *et al.* for their structurally as yet uncharacterized meta–oxoborate polymorphs [28] did not show any correspondence.

Magnetic measurements

The magnetic susceptibilities of polycrystalline, powdered samples $RE(BO_2)_3$ (RE = Dy–Er) were determined with a MPMS SQUID magnetometer (Quantum Design, Inc.) in a temperature range 2 to 300 K with magnetic flux densities up to 5.5 T. The powders were enclosed in silica tubes and fixed at the sample holder rod. The samples were cooled to 2 K in a zero magnetic field and slowly heated to room temperature in the applied external field.

Table 18. Magnetic properties of $RE(BO_2)_3$ (RE = Dy, Ho, Er): μ_{exp}, experimental magnetic moment; Θ, paramagnetic Curie temperature (Weiss constant); M, magnetization at 2 K and 5.5 T; $g \times J$, theoretical saturation magnetization.

Compound	μ_{exp}/μ_B	μ_{exp}/μ_B	Θ [K]	M [μ_B*RE atom^{-1}]	$g \times J$
$Dy(BO_2)_3$	11.1(1)	10.65	−1(1)	6.7(1)	13.3
$Ho(BO_2)_3$	10.2(1)	10.61	−6(1)	5.9(1)	12.5
$Er(BO_2)_3$	9.4(1)	9.58	−10(1)	4.9(1)	10.8

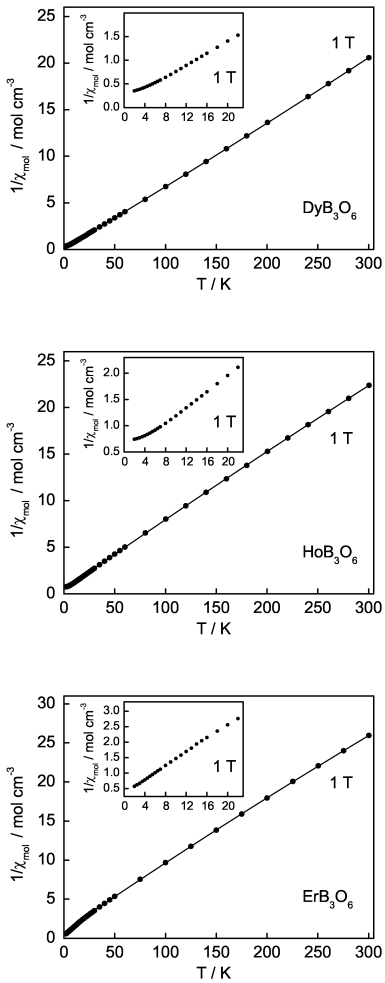

Fig. 9. Temperature dependence of the inverse magnetic susceptibility of $Dy(BO_2)_3$, $Ho(BO_2)_3$, and $Er(BO_2)_3$ measured at an external flux density of 1 T. The low-temperature behaviour is shown in the inserts.

The temperature dependences of the inverse magnetic susceptibilities of $Dy(BO_2)_3$, $Ho(BO_2)_3$ and

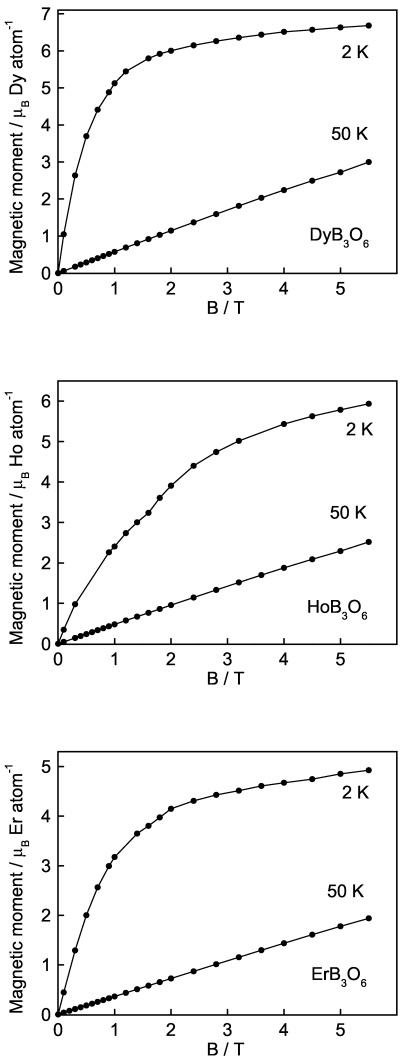

Fig. 10. Magnetization vs. external magnetic flux density of $Dy(BO_2)_3$, $Ho(BO_2)_3$, and $Er(BO_2)_3$ measured at 2 and 50 K.

$Er(BO_2)_3$, measured at an external magnetic flux density of 1 T, are displayed in Fig. 9. The three oxoborates show Curie-Weiss behavior above 50 K with the experimental magnetic moments listed in Table 18. These are close to the theoretical values for the free RE^{3+} ions [78]. The Curie temperatures (Weiss constants) were obtained by extrapolation of the $1/\chi$ *vs* T data to $1/\chi = 0$ (data from 50 K to room temperature). Zero-field and field-cooling measurements have also been carried out from 2 to 40 K at an external flux density of 0.002 T. For all compounds, the zero-field and field-cooling data were rather identical and there was no hint for magnetic ordering. The paramagnetic Curie temperatures (Weiss constants) are slightly negative for the three *meta*-oxoborates, indicating very weak magnetic coupling.

The magnetization *vs* external magnetic field dependence for $Dy(BO_2)_3$, $Ho(BO_2)_3$ and $Er(BO_2)_3$ is linear for 50 K (Fig. 10), as expected for a paramagnetic material. At 2 K, we observe a strong increase of the magnetization with no tendency for saturation in the highest obtainable field of 5.5 T. The experimental magnetizations have reached roughly half of the theoretical $g \times J$ values [78]. Thus, the external field causes a partially parallel spin alignment.

Conclusions

In this paper, we have described the synthesis of the new rare-earth *meta*-oxoborates $RE(BO_2)_3$ (RE = Dy–Lu) *via* multianvil high-pressure techniques from RE_2O_3 (RE = Dy–Lu) and boron oxide B_2O_3. These compounds extend the series of well characterized orthorhombic *meta*-oxoborates [32], which were not attainable under normal-pressure conditions with the exception of $Dy(BO_2)_3$. *In-situ* powder diffraction measurements showed that the substances $RE(BO_2)_3$ (RE = Dy–Er) are stable up to 970 °C, 960 °C, and 940 °C, respectively. The compounds $RE(BO_2)_3$ (RE = Dy–Er) exhibit paramagnetism.

Acknowledgements

We gratefully acknowledge the continous support of these investigations by Prof. Dr. W. Schnick, Department Chemie of the Ludwig-Maximilians-Universität München (Germany). Special thanks go to Dr. P. Mayer and S. Albrecht (LMU-München) for collecting the single-crystal data, to Dipl. Min. S. Schmid for DTA, and to Dipl. Chem. S. Correll (LMU-München) for the *in-situ* powder diffraction measurements. This work was financially supported by the Deutsche Forschungsgemeinschaft, the Fonds der Chemischen Industrie, and the European COST D30 network (D30/003/03).

[1] P. Becker, Adv. Mater. **10**, 979 (1998).
[2] T. Y. Mori, M. Yoshimura, Y. K. Yap, T. Kamimura, Mater. Sci. Eng. **30**, 1 (2000).
[3] D. A. Keszler, Curr. Opin. Solid State Mater. Sci. **1**, 204 (1996).

[4] D. A. Keszler, Curr. Opin. Solid State Mater. Sci. **4**, 155 (1999).
[5] E. M. Levin, R. S. Roth, J. B. Martin, Am. Mineral. **46**, 1030 (1961).
[6] W. F. Bradley, D. L. Graf, R. S. Roth, Acta Crystallogr. **20**, 283 (1966).
[7] J.-Y. Henry, Mater. Res. Bull. **11**, 577 (1976).
[8] R. S. Roth, J. L. Waring, E. M. Levin, Proc. 3rd Conf. Rare Earth Res., Clearwater, Fla. 153 (1963).
[9] G. Chadeyron, M. El-Ghozzi, R. Mahiou, A. Arbus, J. C. Cousseins, J. Solid State Chem. **128**, 261 (1997).
[10] M. Ren, J. H. Lin, Y. Dong, L. Q. Yang, M. Z. Su, L. P. You, Chem. Mater. **11**, 1576 (1999).
[11] K. K. Palkina, V. G. Kuznetsov, L. A. Butman, B. F. Dzhurinskii, Acad. Sci. USSR **2**, 286 (1976).
[12] H. G. Giesber, J. Ballato, W. T. Pennington, J. W. Kolis, Information Sciences **149**, 61 (2003).
[13] H. J. Meyer, Naturwissenschaften **56**, 458 (1969).
[14] H. J. Meyer, A. Skokan, Naturwissenschaften **58**, 566 (1971).
[15] H. J. Meyer, Naturwissenschaften **59**, 215 (1972).
[16] M. Th. Cohen-Adad, O. Aloui-Lebbou, C. Goutaudier, G. Panczer, C. Dujardin, C. Pedrini, P. Florian, R.yD. Massiot, F. Gerard, Ch. Kappenstein, J. Solid State Chem. **154**, 204 (2000).
[17] D. A. Keszler, H. Sun, Acta Crystallogr. **C44**, 1505 (1988).
[18] S. C. Abrahams, J. L. Bernstein, E. T. Keve, J. Appl. Crystallogr. **4**, 284 (1971).
[19] H. Huppertz, Z. Naturforsch. **56b**, 697 (2001).
[20] R. Böhlhoff, H.yU. Bambauer, W. Hoffmann, Z. Kristallogr. **133**, 386, (1971).
[21] S. Lemanceau, G. Bertrand-Chadeyron, R. Mahiou, M. El-Ghozzi, J. C. Cousseins, P. Conflant, R. N. Vannier, J. Solid State Chem. **148**, 229 (1999).
[22] J. Weidelt, H. U. Bambauer, Naturwissenschaften **55**, 342 (1968).
[23] H. Huppertz, B. von der Eltz, J. Solid State Chem. **166**, 203 (2002).
[24] G. Canneri, Gazz. Chim. Ital. **56**, 450 (1926).
[25] J. Weidelt, Z. Anorg. Allg. Chem. **374**, 26 (1970).
[26] I. V. Tananaev, B. F. Dzhurinskii, I. M. Belyakov, Izv. Akad. Nauk SSSR Neorg. Mater. **2**, 1791 (1966).
[27] H. U. Bambauer, J. Weidelt, J. St. Ysker, Z. Kristallogr. **130**, 207 (1969).
[28] I. V. Tananaev, B. F. Dzhurinskii, B. F. Chistova, Izv. Akad. Nauk SSSR Neorg. Mater. **11**, 86 (1975).
[29] G. D. Abdullaev, Kh. S. Mamedov, G. D. Dzhafarov, Sov. Phys. Crystallogr. **20**, 161 (1975).
[30] C. Sieke, T. Nikelski, Th. Schleid, Z. Anorg. Allg. Chem. **628**, 819 (2002).
[31] H. Müller-Bunz, T. Nikelski, Th. Schleid, Z. Naturforsch. **58b**, 375 (2003).
[32] A. Goriounova, P. Held, P. Becker, L. Bohatý, Acta. Crystallogr. Sect. E **59**, i83 (2003).
[33] T. Nikelski, Th. Schleid, Z. Anorg. Allg. Chem. **629**, 1017 (2003).
[34] T. Nikelski, Th. Schleid, personal communication.
[35] L. Li, P. Lu, Y. Wang, X. Jin, G. Li, Y. Wang, L. You, J. Lin, Chem. Mater. **14**, 4963 (2002).
[36] J. H. Lin, S. Zhou, L. Q. Yang, G. Q. Yao, M. Z. Su, J. Solid State Chem. **134**, 158 (1997).
[37] J. H. Lin, L. P. You, G. X. Lu, L. Q. Yang, M. Z. Su, J. Mater. Chem. **8**, 1051 (1998).
[38] J. H. Lin, M. Z. Su, K. Wurst, E. Schweda, J. Solid State Chem. **126**, 287 (1996).
[39] H. Huppertz, B. von der Eltz, J. Am. Chem. Soc. **124**, 9376 (2002).
[40] H. Huppertz, Z. Naturforsch. **58b**, 278 (2003).
[41] H. Emme, H. Huppertz, Z. Anorg. Allg. Chem. **628**, 2165 (2002).
[42] H. Emme, H. Huppertz, Chem. Eur. J. **9**, 3623 (2003).
[43] H. Huppertz, S. Altmannshofer, G. Heymann, J. Solid State Chem. **170**, 320 (2003).
[44] H. U. Bambauer, J. Weidelt, J. S. Ysker, Naturwissenschaften **55**, 81 (1968).
[45] A. Neuhaus, Chimia **18**, 93 (1964).
[46] H. Huppertz, Z. Naturforsch. **58b**, 257 (2003).
[47] D. Walker, M. A. Carpenter, C. M. Hitch, Am. Mineral. **75**, 1020 (1990).
[48] D. Walker, Am. Mineral. **76**, 1092 (1991).
[49] D. C. Rubie, Phase Trans. **68**, 431 (1999).
[50] J. W. Visser, J. Appl. Crystallogr. **2**, 89 (1969).
[51] $\mathrm{WinX}^{\mathrm{POW}}$ Software, STOE & CIE GmbH, Darmstadt (1998).
[52] W. Herrendorf, H. Bärnighausen, HABITUS, Program for Numerical Absorption Correction, University of Karlsruhe / Giessen, Germany (1993 / 1997).
[53] G. M. Sheldrick, SHELXS-97, Program for the Solution of Crystal Structures, University of Göttingen, Germany (1997).
[54] G. M. Sheldrick, SHELXL-97, Program for Crystal Structure Refinement, University of Göttingen, Germany (1997).
[55] W. E. Klee, Z. Kristallogr. **179**, 67 (1987).
[56] A. Beukemann, W. E. Klee, Z. Kristallogr. **209**, 709 (1994).
[57] A. Beukemann, W. E. Klee, Z. Kristallogr. **201**, 37 (1992).
[58] G. Thimm, S. Schumacher, W. Uhr, W.yE. Klee, TOPOLAN – Topological Analysis of Crystal Structures, University of Karlsruhe, Germany (1993).
[59] F. C. Hawthorne, P. C. Burns, J. D. Grice, Boron: Mineralogy, Petrology, and Geochemistry, Chapter 2, Reviews in Mineralogy 33, Mineralogical Society of America, Washington (1996).

[60] I. D. Brown, D. Altermatt, Acta Crystallogr. Sect. B **41**, 244 (1985).
[61] N. E. Brese, M. O'Keeffe, Acta Crystallogr. Sect. B **47**, 192 (1991).
[62] R. Hoppe, S. Voigt, H. Glaum, J. Kissel, H. P. Müller, K. Bernet, J. Less-Common Met. **156**, 105 (1989).
[63] R. Hoppe, Angew. Chem. **78**, 52 (1966); Angew. Chem. Int. Ed. **5**, 95 (1966).
[64] R. Hoppe, Angew. Chem. **82**, 7 (1970); Angew. Chem. Int. Ed. **9**, 25 (1970).
[65] R. Hübenthal, MAPLE, Program for the Calculation of MAPLE Values, Vers. 4, University of Giessen, Germany (1993).
[66] C. T. Prewitt, R.D. Shannon, Acta Crystallogr. Sect. B **24**, 869 (1968).
[67] M. Ren, J. H. Lin, Y. Dong, L. Q. Yang, M. Z. Su, L. P. You, Chem. Mater. **11**, 1576 (1999).
[68] J. P. Laperches, P. Tarte, Spectrochim. Acta **22**, 1201 (1966).
[69] G. Blasse, G. P. M. van den Heuvel, Phys. Stat. Sol. **19**, 111 (1973).
[70] W. C. Steele, J. C. Decius, J. Chem. Phys. **25**, 1184 (1956).
[71] R. Böhlhoff, H. U. Bambauer, W. Hoffmann, Z. Kristallogr. **133**, 386 (1971).
[72] K. Machida, H. Hata, K. Okuno, G. Adachi, J. Shiokawa, J. Inorg. Nucl. Chem. **41**, 1425 (1979).
[73] H. Huppertz, G. Heymann, Solid State Sci. **5**, 281 (2003).
[74] M. Touboul, N. Penin, G. Nowogrocki, J. Solid State Chem. **150**, 342 (2000).
[75] C. E. Weir, R. A. Schroeder, J. Res. Nat. Bur. Stand. **86A,** 465 (1964).
[76] A. Perloff, S. Block, Acta Crystallogr. **20**, 274 (1966).
[77] D. L. Corker, A. M. Glazer, Acta Crystallogr. **B52**, 260 (1996).
[78] H. Lueken, Magnetochemie, Teubner, Stuttgart (1999).